



Measurement of the inclusive $t\bar{t}$ production cross section in $p\bar{p}$ collisions at $\sqrt{s} = 1.96$ TeV

The D0 collaboration
(Dated: July 27, 2015)

The inclusive cross section of top quark-antiquark pairs produced in $p\bar{p}$ collisions at $\sqrt{s} = 1.96$ TeV is measured with data in lepton+jets and dilepton final states. The data sample corresponds to 9.7 fb^{-1} of integrated luminosity recorded with the D0 detector during Run II of the Fermilab Tevatron Collider. We select lepton+jets events containing an isolated high- p_T lepton, a large imbalance in transverse momentum, and two or more jets. Dilepton final states are selected by requiring two isolated high- p_T leptons, a large imbalance in transverse momentum, and one or more jets. We perform two cross section measurements and a combination of those: in the lepton+jets decay channel we exploit topological variables and the multivariate output discriminant of the b -jet identification combined in a multivariate analyses and in the dilepton decay channel we employ the multivariate output discriminant of the b -jet identification. For a top quark mass of 172.5 GeV, we measure a combined inclusive top quark-antiquark pair production cross section of:

$$\sigma_{t\bar{t}} = 7.73 \pm 0.13 \text{ (stat.)} \pm 0.55 \text{ (syst.) pb,}$$

which is consistent with standard model predictions. We also perform a likelihood fit to the measured and predicted top quark mass dependence of the inclusive cross section, which yields a measurement of the pole mass of the top quark. The extracted value is: $169.5^{+3.3}_{-3.4}$ (tot.) GeV.

I. INTRODUCTION

The top quark, discovered by the CDF and D0 experiments in 1995 [1, 2], is the heaviest of all elementary particles in the standard model (SM), with a mass of 174.3 ± 0.7 GeV [3]. The production of top quark-antiquark pairs ($t\bar{t}$) at the Fermilab Tevatron Collider is dominated by the quark-antiquark ($q\bar{q}$) annihilation process. The measurement of inclusive $t\bar{t}$ production cross sections provides a direct test of quantum chromodynamics (QCD), the theory of the strong interaction. Inclusive $t\bar{t}$ production cross sections have been previously measured at the Tevatron [4, 5] and the LHC [6, 7]. Compared to the previous D0 result [4], the current measurement employs nearly a factor of two more data and a refined analysis technique allowing for higher precision tests of perturbative QCD (pQCD). We determine the pole mass of the top quark from the top quark mass dependence of the inclusive $t\bar{t}$ production cross section, so as to get a theoretically well defined top quark mass.

Events are selected in the lepton+jets (ℓ +jets) and dilepton decay channels, where the lepton (ℓ) refers to either an electron or a muon. These channels corresponds to $t\bar{t} \rightarrow W^+bW^-\bar{b}$ decays, where in the ℓ +jets channel one of the two W bosons decays leptonically ($W \rightarrow \ell\nu$) while the other W boson decays hadronically ($W \rightarrow q\bar{q}'$). In the dilepton decay channel both W bosons decay leptonically. Both decay channels include small contributions from electrons and muons stemming from the decay of τ leptons ($t \rightarrow Wb \rightarrow \tau\nu_\tau b \rightarrow \ell\nu_\ell\nu_\tau b$). The details of the event selection in the two decay channels are discussed in section V.

II. MEASUREMENT STRATEGY

This measurement uses various Multi Variate Analysis (MVA) techniques [8], as implemented in TMVA [9], in order to measure the inclusive cross section in the ℓ +jets and dilepton decay channels. For the dilepton decay channel we make use of the output distribution of the MVA that D0 uses to identify jets that are likely to originate from b quarks (b -tagged jets) [10]. This method is superior to a simple cut-and-count since each $t\bar{t}$ event contains two true b -quarks from the decays of top quarks, and we refer to that method in the following as “MVA b -jet method”. We construct a topological discriminant for events in the ℓ +jets decay channel to make the best use of the distinct kinematic structure of top quark events along with b -tagging information, and in the following referred to as “MVA topological method”. The details of these methods are described in Sec. VII A. We combine the results of the MVA b -jet method in the dilepton decay channel with the ones provided by the MVA topological method in the ℓ +jets decay channel in order to get a combined inclusive $t\bar{t}$ cross section measurement.

III. MONTE CARLO SIMULATIONS AND QCD PREDICTIONS

Monte Carlo simulations are used to model the reconstruction of the observables, to estimate systematic uncertainties associated with the measurements, and to simulate physics processes. Different MC event generators are used to implement hard scattering processes based on leading-order (LO) and next-to-leading order (NLO) QCD calculations, and are complemented with parton shower evolution. To simulate detector effects, generated events (including hadronization) are passed through a detailed simulation of the D0 detector based on GEANT [11]. To account for effects from additional overlapping $p\bar{p}$ interactions, events without any trigger requirements are selected randomly in collider data and overlaid on the fully simulated MC events.

The $t\bar{t}$ samples are generated with MC@NLO version 3.4 [12] or with ALPGEN version 2.11 [13], both produce only on-shell top quarks. Single top quark production ($q\bar{q}' \rightarrow t\bar{b}, q'g \rightarrow tq\bar{b}$) is modeled using COMPHEP [14]. For events generated with MC@NLO, the parton showering is performed with HERWIG version 6.510 [15], whereas for ALPGEN and COMPHEP parton showering is implemented by PYTHIA version 6.409 [16]. The parton distribution functions (PDF) choice made in generating MC events is CTEQ6L1 [17], with the exception of MC@NLO and the t -channel single top process, where CTEQ6M [18] PDFs are used. For all the MC simulations involving the generation of top quarks, a top quark mass of $m_t = 172.5$ GeV is used. The difference with the current Tevatron top quark mass combination of 174.3 GeV [3] has negligible impact on the analysis. For the $t\bar{t}$ ℓ +jets ($\ell\ell$) decay channel the branching fraction B of 0.342 ± 0.004 (0.04 ± 0.001) [43] is used, respectively. These values include electrons and muons originating from the decay of τ leptons ($\tau_\ell \rightarrow \ell\nu_\ell\nu_\tau$).

Several QCD predictions for inclusive $t\bar{t}$ cross sections have been calculated at higher orders than those included in the MC generators. The fully resummed NNLO QCD calculation (using $m_t = 172.5$ GeV), finds $\sigma_{\text{tot}}^{\text{res}} = 7.35_{-0.27}^{+0.23}$ (scale + pdf) pb [19]. An approximate next-to-next-to-next-to-leading order (aNNNLO) calculations for $m_t = 173$ GeV finds $\sigma_{\text{tot}}^{\text{res}} = 7.37 \pm 0.39$ (scale + pdf) pb [20]. Both use the MSTW2008NNLO PDF [21] and the scale used to calculate the inclusive cross section is set to m_t .

A. Modeling of background contributions in the ℓ +jets decay channel

The main background to $t\bar{t}$ production in the ℓ +jets decay channel is the production of a W plus jets (W +jets). It consists of events where one W boson is produced via an electroweak interaction, together with additional partons from QCD processes. The W +jets final state can be split into four subsamples according to parton flavor: $Wb\bar{b}$ +jets, $Wc\bar{c}$ +jets, Wc +jets and W +light jets (Wlp +jets), where light refers to gluons, u , d or s quarks. The W +jets contribution dominates especially in the lower jet bin multiplicities. The LO ALPGEN cross sections are corrected for NLO effects as provided by MCFM [22]: the W +jets cross section is multiplied by 1.30, and the cross sections of W heavy flavor (WHF) processes are multiplied by an additional scale factor s^{WHF} of 1.47 for $Wb\bar{b}$ +jets and $Wc\bar{c}$ +jets and 1.27 for Wc +jets. Apart from these theoretical corrections we constrain the absolute normalization by employing the data as described later in Section VI. The p_T distribution of the W boson in MC simulation is reweighted to match the p_T distribution of the Z boson measured in D0 data [23] multiplied by the SM ratio of these two distributions, which was calculated at NLO using RESBOS [24].

The second most dominant background contribution is due to multijet processes where a jet is misidentified as an electron in the e +jets channel, or where a muon originating from the semileptonic decay of a heavy hadron appears to be isolated in the μ +jets channel. More details and a brief discussion on the determination of the multijet background is given in Sec. VI.

Other backgrounds include events from Z/γ^* +jets production, which includes Z bosons and virtual photons (γ^*) decaying to electron, muon, or tau pairs. The LO ALPGEN predictions are similarly corrected using the NLO calculation of MCFM. The Z/γ^* +jets cross section is multiplied by 1.30, whereas the heavy flavor component of the Z/γ^* +jets cross sections ($(Z/\gamma^*c\bar{c} + Z/\gamma^*b\bar{b})$ +jets) by an additional 1.67 and 1.52, respectively. The simulated p_T distribution of the Z boson is reweighted to match the measured p_T distribution in $Z \rightarrow \ell\ell$ [23].

The single top quark background consists of s - and t -channel single top quark production, which are normalized to the NLO cross sections of 1.04 and 2.26 pb [25], respectively. As the single top quark background yields only a few events passing all selection criteria described later, no effects are considered from the dependence of this background on m_t .

Diboson production (WW , WZ and ZZ bosons) processes are normalized to NLO cross sections, calculated with MCFM, of 11.62 pb, 3.25 pb and 1.33 pb, respectively.

B. Modeling of background contributions in the $\ell\ell$ decay channel

The backgrounds in the dilepton decay channel are in general smaller compared to the ℓ +jets decay channel. The dominant source originates from Z/γ^* +jets production, followed by events from diboson production. For both processes the modeling employs the same implementation as described previously for the ℓ +jets decay channel.

The third most dominant source of backgrounds are multijet events, with the determination briefly summarized in Sec. VI.

IV. THE D0 DETECTOR

The D0 detector [26] consists of several subdetectors designed for identification and reconstruction of the products of $p\bar{p}$ collisions. A silicon microstrip tracker (SMT) [27, 28] and central fiber tracker surround the interaction region for pseudorapidities¹ $|\eta| < 3$ and $|\eta| < 2.5$, respectively. These elements of the central tracking system are located within a superconducting solenoidal magnet generating a 2 T field, providing measurements for reconstructing event vertices and trajectories of charged particles. The SMT allows for a precision of 40 μm or better for the reconstructed primary $p\bar{p}$ interaction vertex (PV) in the plane transverse to the beam direction. The impact parameter of typical charged particle trajectories relative to the PV is determined with a precision between 20 and 50 μm depending on the number of SMT hits and particle momenta. The impact parameter and its measurement uncertainty are key components of lifetime-based identification of jets containing b quarks. Particle energies are measured using a liquid argon sampling calorimeter that is segmented into a central calorimeter covering $|\eta| < 1.1$, and two end calorimeters extending the coverage to $|\eta| = 4.2$. Outside of the calorimetry, trajectories of muons are measured using three layers of tracking detectors and scintillation trigger counters, and an iron toroidal magnet generating a 1.8 T field between

¹ The pseudorapidity $\eta = -\ln[\tan(\theta/2)]$ is measured relative to the center of the detector, and θ is the polar angle with respect to the proton beam direction. The z -axis is pointing along the proton beam direction.

the first two layers [29]. Plastic scintillator arrays are located in front of the end-calorimeter cryostats to measure the luminosity [30]. The trigger and data acquisition systems are designed to accommodate the high luminosities of Run II [31].

V. EVENT SELECTION

This analysis is based upon the full Run II data sample recorded by the D0 detector at $\sqrt{s} = 1.96$ TeV. After applying data quality requirements, the data correspond to an integrated luminosity of 9.7 fb^{-1} . The general selection criteria applied to both the ℓ +jets and dilepton decay channels are summarized in the following list.

1. $|z_{PV}| < 60$ cm of the center of the detector along the beam axis.
2. Number of tracks associated with the primary vertex greater or equal to 3.
3. After correcting the energy of the jet to the particle level [32] only jets with a transverse momentum $p_T > 20$ GeV and $|\eta| < 2.5$ are selected.
4. Jets which satisfy the b -tagging requirement are required to have at least two tracks coming from the PV. More details for the individual decay channels are provided below.
5. Identified leptons [33, 34] are required to originate from the PV by demanding $|\Delta z(\ell, PV)| < 1$ cm.
6. To ensure that leptons are isolated, a distance $\Delta R = \sqrt{(\Delta\eta)^2 + (\Delta\phi)^2}$ between a lepton and a jet of $\Delta R(\ell, \text{closest jet}) > 0.5$ is required.

Measurements in both decay channels require jets identified as originating from a b -quark by identifying them as b -jet candidates (b -tagged) with a multivariate discriminant. The discriminant combines variables that characterize the presence and properties of secondary vertices and tracks within jets. We do not impose any requirements on this discriminant but directly employ it to measure the inclusive cross section as described in Sec. VII.

A. Event selection in the ℓ +jets decay channel

The selection requirements for the cross section measurement for the ℓ +jets channel are very similar to the ones described in Ref. [35] and are summarized briefly in the following list.

1. Exactly one isolated lepton with a transverse momentum $p_T > 20$ GeV and $|\eta| < 1.1$ (for electrons) or $|\eta| < 2$ (for muons) is required. Events with more than one lepton are rejected.
2. The measurement of \cancel{E}_T is based on calorimetry, not including charged track momenta and we require $\cancel{E}_T > 20$ GeV.
3. For the μ +jets sample we remove misreconstructed muons by requiring upper limits on the transverse mass of the reconstructed W boson of $M_T^W < 250$ GeV and $\cancel{E}_T < 250$ GeV. To further remove such events, we employ an additional requirement on the significance of the track curvature \mathcal{S}_c described in more detail in Ref. [35].
4. To reduce multijet background we require a minimum separation between the direction of the lepton and the direction of the missing momentum [35]: $\Delta\phi(e, \cancel{E}_T) > 2.2 - 0.045 \cdot \cancel{E}_T/\text{GeV}$ and $\Delta\phi(\mu, \cancel{E}_T) > 2.1 - 0.035 \cdot \cancel{E}_T/\text{GeV}$.
5. At least two jets are required. To suppress jets from additional collisions, jets are required to contain two tracks consistent with originating from the PV.
6. The trigger requirement is a logical “OR” of the condition for at least “one lepton” and for at least “a lepton and a jet”.

B. Event selection in the dilepton decay channel

Apart from the general selection requirements discussed in the opening of this section, additional requirements specific to the dilepton channel are made. The selection requirements for this cross section measurement are very similar to the ones used for the leptonic asymmetry measurements in the dilepton channel published earlier [36] and are summarized briefly in the following list.

1. Electrons are required to have a transverse momentum of $p_T > 15$ GeV and $|\eta| < 2.5$. We exclude the $1.1 < |\eta| < 1.5$ region.
2. Muons are selected with at least 15 GeV and $|\eta| < 2$. To remove misreconstructed muons we require muons with $p_T < 200$ GeV for the dimuon channel.
3. For the $e\mu$ channel exactly one electron and one or more muons are identified as above. In addition at least one jet as described further above is required.
4. For the $\mu\mu$ channel two or more muons are identified as above. In addition at least two jets as described further above is required.
5. For the ee channel two or more electrons are identified as described above. In addition at least two jets as described further above is required.
6. The two selected leptons should have opposite charges. If more than one lepton pair is found, the lepton pair with the largest p_T scalar sum is chosen.
7. Distance in z between the two selected lepton tracks $|z_{\ell_1} - z_{\ell_2}|$, should be less than 2 cm. These z -values are for extrapolated tracks, which have closest approach to the beam line.
8. Additional quality requirements are imposed to remove background from bremsstrahlung. To further reduce contributions from background, additional topological requirements based on \cancel{E}_T , \cancel{E}_T significance and H_T are imposed. The details are described in Ref. [36].
9. In the $e\mu$ channel, no explicit trigger requirement is applied, whereas in the ee or $\mu\mu$ channel the single lepton trigger is required.

VI. SAMPLE COMPOSITIONS

We distinguish between instrumental backgrounds and irreducible backgrounds from processes with final states similar to $t\bar{t}$. Instrumental backgrounds are due to multijet processes where one or more jets are misidentified as an electron, or where one or more muons originating from the semileptonic decay of a heavy hadron appear to be isolated. Systematic uncertainties on the determination of the sample composition are discussed in Sec. X A 4.

A. Determination of the ℓ +jets sample composition

The irreducible background processes are estimated using MC simulations described in Sec. III. Most of this background arises from W +jets production especially in the 2 jet multiplicity bin. The W +jets cross section is scaled in each jet multiplicity bin separately by a W +jets heavy-flavor scale factor $s_{\text{fit}}^{\text{WHF}}$ to match the number of data events after subtraction of all other instrumental and irreducible background processes as well as the signal process.

Data-driven and MC methods are combined in the “matrix method” [4, 37], which is employed to model the instrumental background originating from multijet (MJ) processes. The MJ contribution is determined from an orthogonal data sample by requiring $\cancel{E}_T < 10$ GeV and exact same selection criteria for the electron or muon and the jets. This data sample is enriched in MJ events and no real isolated leptons are assumed to be included. We determine the shape and absolute contribution of multijet events in bins of jet multiplicity by comparing this data sample with one that has looser lepton criteria but the same \cancel{E}_T requirement.

Figure 1 demonstrates the quality of the modeling of the selected events in the ℓ +jets sample with the background and signal contributions, using a theoretical inclusive $t\bar{t}$ cross section of 7.48 pb [38]. The expected composition of the sample after the final selection is given in Table I.

TABLE I: Expected number of events with at least two jets due to each process. Uncertainties are statistical and systematical added in quadrature, see Section X A 4 for details on systematic uncertainties related to the sample composition. Events in the dilepton decay channel are denoted by $\ell\ell$.

Process	ℓ +jets decay channel											
	$e + 2$ jets		$e + 3$ jets		$e + \geq 4$ jets		$\mu + 2$ jets		$\mu + 3$ jets		$\mu + \geq 4$ jets	
Multijet	9160	± 2350	2266	± 550	464	± 120	1546	± 630	418	± 170	99	± 40
Single top	471	± 60	129	± 20	27	± 5	331	± 40	92	± 10	20	± 3
Wlp +jets	37937	$^{+1350}_{-700}$	5544	$^{+200}_{-100}$	850	$^{+30}_{-20}$	32701	$^{+1150}_{-600}$	5313	$^{+200}_{-100}$	835	$^{+30}_{-15}$
$(Wc\bar{c} + Wb\bar{b})$ +jets	6020	$^{+1000}_{-1400}$	1502	$^{+250}_{-350}$	329	$^{+60}_{-80}$	4998	$^{+850}_{-1150}$	1391	$^{+250}_{-300}$	315	$^{+50}_{-70}$
Z/γ^*lp +jets	2031	± 400	390	± 80	57	± 10	2557	± 500	422	± 80	49	± 10
$(Z/\gamma^*c\bar{c} + Z/\gamma^*b\bar{b})$ +jets	369	± 70	114	± 20	24	± 5	485	± 100	120	± 20	21	± 5
Diboson	1926	± 140	338	± 20	52	± 5	1417	± 100	249	± 20	40	± 5
$t\bar{t}, \ell\ell$	566	± 30	182	± 10	31	± 5	345	± 20	118	± 10	22	± 5
\sum bgs	58479	± 2900	10465	± 650	1834	± 140	44381	± 1650	8123	± 350	1402	± 80
$t\bar{t}, \ell$ +jets	669	± 30	1460	± 70	1177	± 60	393	± 20	1002	± 50	909	± 50
\sum (sig + bgs)	59148	± 2900	11925	± 650	3011	± 140	44773	± 1650	9125	± 350	2310	± 80
Data	59122		11905		3007		44736		9098		2325	

B. Determination of the $\ell\ell$ sample composition

The main backgrounds in the dilepton final state originate from $Z \rightarrow \ell\ell$, instrumental backgrounds, and diboson production (WW , WZ , ZZ). The $Z \rightarrow \ell\ell$ and diboson backgrounds are evaluated from MC as described in Section III B, whereas the instrumental background use a mixture of MC and data-driven approaches as described below.

Instrumental backgrounds in the $\ell\ell$ channel come from multijet and W +jets events, where one or two jets are misreconstructed as an electron or where a muon from a jet passes the isolation criteria and is identified as a final state muon. Similarly as in the ℓ +jets channel the contribution from these backgrounds are estimated directly from data using the matrix method separately for the ee and $e\mu$, whereas the “same-sign method” is employed in the $\mu\mu$ channel [39]. The contribution in each of those channels is derived from an orthogonal data sample by requiring that the two leptons have the same charge but otherwise the same selection criteria as for $t\bar{t}$ events as was done in [39].

The yields after applying the described selection are given in Table II for the individual channels.

TABLE II: Expected number of events in the $ee + \geq 2$ jets, $\mu\mu + \geq 2$ jets, $e\mu + 1$ jets and $e\mu + \geq 2$ jets due to each process (uncertainties are statistical only).

Process	dilepton decay channel							
	$ee + \geq 2$ jets		$\mu\mu + \geq 2$ jets		$e\mu + 1$ jets		$e\mu + \geq 2$ jets	
Multijet	5.7	$^{+0.3}_{-0.3}$	7.0	$^{+3.1}_{-2.4}$	28.3	$^{+5.1}_{-5.1}$	32.5	$^{+5.6}_{-5.6}$
$Z \rightarrow \ell\ell$	66.6	$^{+12.0}_{-11.0}$	107.6	$^{+15.1}_{-14.9}$	74.6	$^{+5.2}_{-5.2}$	57.5	$^{+7.7}_{-6.9}$
Diboson	9.9	$^{+2.3}_{-2.2}$	12.6	$^{+2.7}_{-2.8}$	38.5	$^{+2.2}_{-2.2}$	14.7	$^{+3.3}_{-3.2}$
$t\bar{t}, \ell\ell$	107.7	$^{+10.8}_{-9.7}$	101.5	$^{+8.1}_{-5.4}$	86.5	$^{+7.7}_{-5.7}$	313.7	$^{+26.3}_{-19.1}$
\sum (sig + bgs)	190	$^{+20}_{-19}$	229	$^{+20}_{-19}$	228	$^{+13}_{-12}$	418	$^{+31}_{-25}$
Data	215		242		236		465	

Figure 2 demonstrates the quality of the modeling of the selected events in the $\ell\ell$ sample with the background and signal contributions, using a theoretical inclusive $t\bar{t}$ cross section of 7.48 pb.

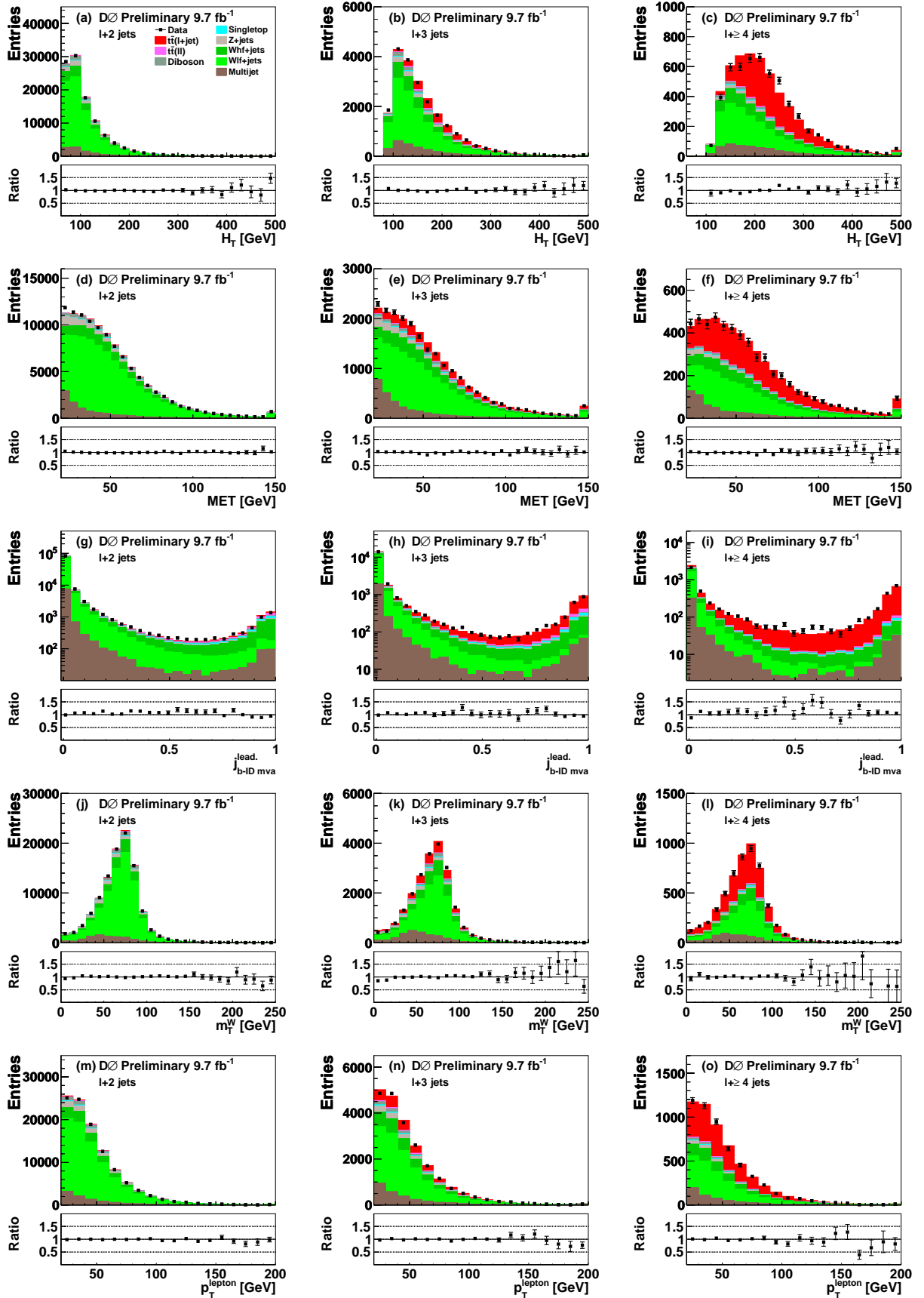


FIG. 1: (color online) Distributions of (a)–(c) the scalar sum of the p_T values of the lepton and jets, (d)–(f) \cancel{E}_T , (g)–(i) $j_{b\text{-ID}}^{\max}$, (j)–(l) the transverse mass of the reconstructed W boson candidate m_T^W , and (m)–(o) p_T^{lepton} for the ℓ +jets final state in the 2 jet, 3 jet and inclusive 4 jet multiplicity bin. The data are compared to the sum of predicted contributions from signal and background processes, using the theoretical value of the inclusive $t\bar{t}$ cross section of 7.48 pb. The highest bin in the histograms is used as an overflow bin. The ratios of data to the sum of the signal and all background contributions are shown in the panels below the distributions.

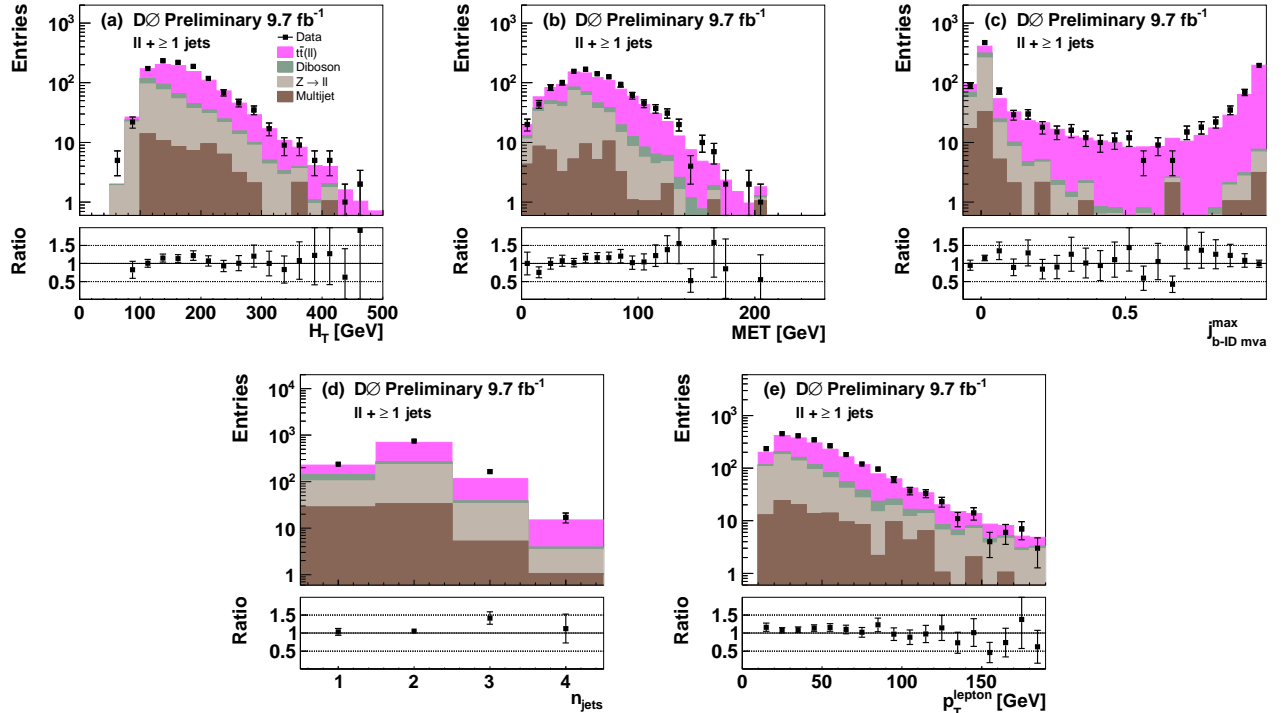


FIG. 2: (color online) Distributions of (a) the scalar sum, H_T , of the p_T values of the lepton and jets, (b) \cancel{E}_T , (c) j_{b-ID}^{max} MVA, (d) the number of jets, and (e) lepton p_T for ll final states with at least 1 jet. The data are compared to the sum of predicted contributions from signal and background processes, using the initial value of the measured inclusive $t\bar{t}$ cross section of 7.48 pb. The highest bin in the histograms is used as an overflow bin. The ratios of data to the sum of the signal and all background contributions are shown in the panels below the distributions.

VII. MULTIVARIATE MEASUREMENT TECHNIQUES

The inclusive $t\bar{t}$ cross section $\sigma(t\bar{t})$ is measured by employing two different techniques, all of them based on MVA techniques as introduced in Sec. II. We use different discriminant output distributions of decision trees in order to separate the signal from the background. The event sample is subsequently split into smaller samples or “branches”, in principle until each event ends up in his own mutually exclusive category. At each splitting point the separation is optimized by employing training samples for the signal and background contributions. The output or discriminant value provides the probability of an event to be signal like. We use all background contributions in the training process and verify that there is no bias due to overtraining of the method.

In particular we employ decision trees with an additional weight to improve the signal to background separation, called “boosted decision trees” (BDT). A better performance is achieved when a slightly modified technique is chosen, which enhances weak classifiers in the training process, called “boosted decision trees with gradients” (BDTG). For the measurement of the $t\bar{t}$ production cross section in this paper we employ the BDTG method. A comparison of the signal to background separation of the BDT and BDTG method is given later in this Section.

In the $l+jets$ decay channel the MVA topological method is carried out (see Section VII A), whereas for the dilepton channel the MVA b -jet method is used as explained in Section VII B. These measurements are based on a fit of the predicted number of signal $t\bar{t}$ and background events to the observed number of events in data. Results presented are the MVA topological method in the $l+jets$ decay channel, the MVA b -jet method in the dilepton channel, and the combination of both decay channels using these results.

In order to measure the cross section we perform a log-likelihood profile fit of Monte Carlo (MC) simulation templates to data using a nuisance parameter for every source of systematic uncertainty as described in Sec. XI. The $l+jets$ channel has a large fraction of background contributions with larger systematic uncertainties. In order to get reasonable initial values for the log-likelihood profile fit, as described in Sec. X A 4, we first perform a simultaneous fit of the $\sigma(t\bar{t})$, the $(Wc\bar{c} + Wb\bar{b})+jets$, and the $Wlp+jets$ contributions.

A. MVA methods in the ℓ +jets channel

Events in the ℓ +jets channel are separated into samples according to the lepton type and the number of jets, $n_{\text{jet}} = 2, 3, \geq 4$, which results into 6 different channels. In order to build a topological discriminant, a total of 50 variables were analyzed. The individual distributions are verified to have a good modeling of the data by the MC by means of the Kolmogorov-Smirnov (KS) test and a χ^2 test. The KS test is based on differences between empirical distribution functions (EDFs) of two samples. We exclude all variables with poor modeling of the data, which at the same time have only little separation power between signal and background. Depending on the jet multiplicity bin a total of about 30 variables is selected as input to the MVA topological method. In particular we include the maximum output value of the MVA b -jet discriminant for the leading jet in our topological discriminant, since it shows superior performance as discussed in the next section. Adding more variables has a negligible effect on the signal to background separation of the MVA topological method. All selected variables are defined in appendix A and serve as the input variables for the MVA topological method.

Figure 3 shows the separation of signal and background in the ℓ +jets decay channel using as an example the exactly three jet multiplicity bin of the e +jets channel. The performance of the μ +jets channel and other jet multiplicity bins is very similar. We compare the MVA topological method as described in Sec. VII A, a topological method excluding any b -jet information but otherwise exactly the same information (MVA no- b -ID-topological method), both of these methods are implemented as BDT and BDTG as introduced earlier in this section. For comparison we also show the pure MVA b -jet method in the ℓ +jets channel. For most values of the true identification rate the MVA b -jet method has a smaller fake identification rate as the MVA no- b -ID-topological method, but at true identification rate values of about 85% the MVA no- b -ID-topological method surpasses the MVA b -jet method. Compared to these two MVA methods the MVA topological method shows superior behaviour with an area under the curve increased by 6 – 10%. In particular we choose BDTG since it provides a further small improvement over the BDT method.

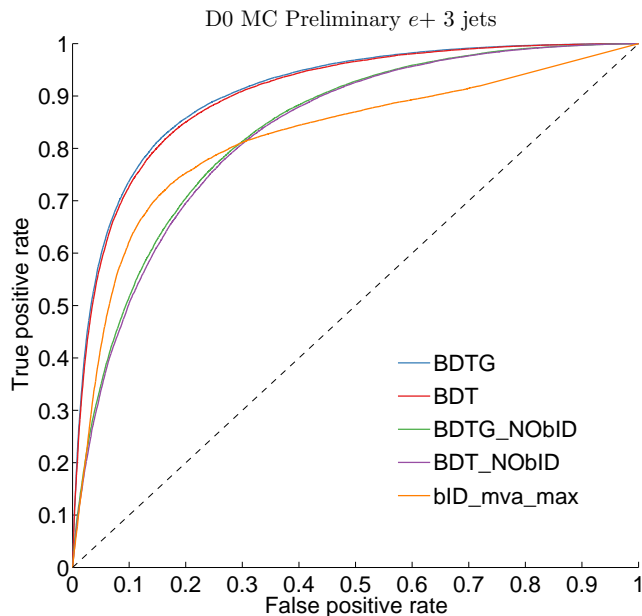


FIG. 3: (color online) Comparing the different measurement techniques in terms of their signal to background rejection capabilities. More details can be found earlier in Section VII.

B. MVA b -jet method in the $\ell\ell$ channel

The MVA value of the jet with highest MVA discriminant output value $j_{b\text{-ID MVA}}^{\text{max}}$ in the event is normally employed to b -tag jets, but in this measurement it is used to measure the $t\bar{t}$ production cross section in the $\ell\ell$ channel. Events in the dilepton channel are separated into samples according to the lepton type and the number of jets. Due to the small background contribution and the size of the signal contribution in the dilepton channel, a separation of channels in terms of b -tagged jets is not applied.

VIII. OUTPUT DISTRIBUTIONS OF THE MVA TOPOLOGICAL METHOD IN THE ℓ +JETS CHANNEL

Figure 4 shows the MVA output distributions of the topological method using an expected $t\bar{t}$ cross section of 7.48 pb. The e +jets channel is shown in Fig. 4(a) – (c) for the two, three and inclusive four jet multiplicity bin, whereas (d) – (f) shows the two, three and inclusive four jet multiplicity bin for the μ +jets channel.

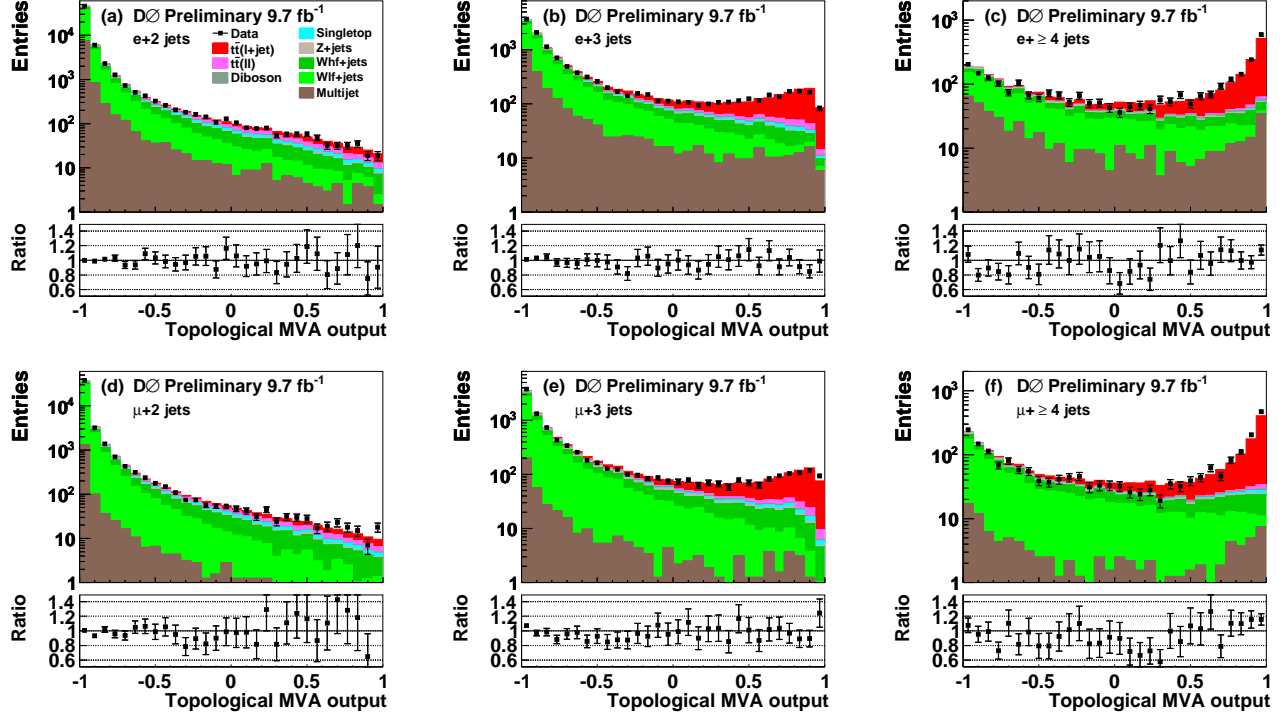


FIG. 4: Pre-fit MVA topological discriminant distributions using the theoretical $t\bar{t}$ cross section for the (a) – (c) e +jets channel and for the (d) – (f) μ +jets channel in the two, three and inclusive four jet multiplicity bin. Only statistical uncertainties of the data are shown.

IX. OUTPUT DISTRIBUTIONS OF THE MVA b -JET METHOD IN THE $\ell\ell$ CHANNEL

The shape of the MVA output distributions in the dilepton channel allows one to distinguish between $t\bar{t}$ events located at high output values and the most dominant Z/γ^*+jets background contribution located at low output values. Data and MC templates in the dilepton channel are separated into four channels with respect to lepton type and number of jets. For $e\mu$ exactly 1 and ≥ 2 jets are required, whereas for ee and $\mu\mu$ only the ≥ 2 jet bin is used. The MVA output distributions of the b -ID MVA method given by the jet with the leading value, j_{b-ID}^{max} , is used to measure the cross section are shown in Figure 5 for (a) $e\mu$ events with exactly one jet, (b) $e\mu$ events with at least 2 jets, (c) ee events with at least 2 jets and (d) $\mu\mu$ events with at least 2 jets. An expected $t\bar{t}$ cross section of 7.48 pb is used.

X. SYSTEMATIC UNCERTAINTIES

Systematic uncertainties are assessed by varying the values of a specific parameter in the modeling of the data, and determining the effect on the distributions or MC templates of the MVA topological method or the b -ID MVA method. Unless otherwise stated, the magnitude of the parameter modifications is obtained from alternative calibrations of the MC simulation. The nominal MVA distributions and the modified ones are both employed to measure the $t\bar{t}$ production cross section in the two decay channels. The modified MC templates represent the systematic uncertainties, which

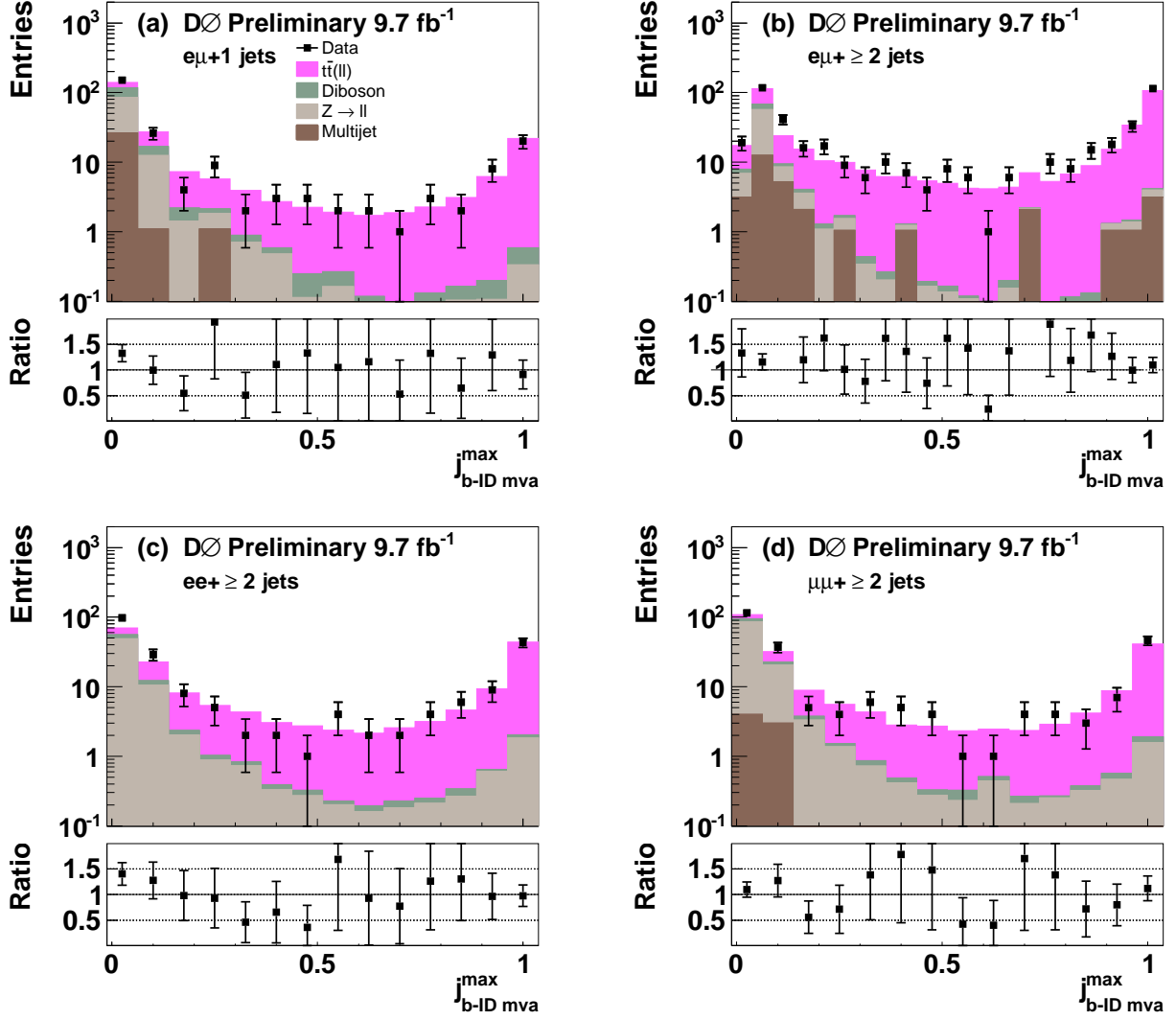


FIG. 5: The MVA output distributions of the b -ID MVA method given by the jet with the leading value, $j_{b\text{-ID MVA}}^{\max}$, for (a) $e\mu$ events with exactly one jet, (b) $e\mu$ events with at least 2 jets, (c) ee events with at least 2 jets and (d) $\mu\mu$ events with at least 2 jets are shown.

are constrained together with the nominal MC template by means of a simultaneous fit as described in Sec. XI and Sec. XII.

A. The ℓ +jets channel

In the following we describe the sources of systematic uncertainties studied in the ℓ +jets channel. As discussed above each source of systematic uncertainty yields a modified discriminant distribution of the MVA topological method and is used as a nuisance parameter in a simultaneous fit to determine the $t\bar{t}$ production cross section in the ℓ +jets channel (see Section XI). The pre-fit systematic uncertainties are summarized in Table III, whereas the post-fit effects of the systematic uncertainties are summarized in Table IV.

1. *Modeling of signal*

The effect of an alternative signal model for $t\bar{t}$ production is estimated by comparing $t\bar{t}$ events generated with MC@NLO+HERWIG to those from ALPGEN+HERWIG. Comparing ALPGEN+PYTHIA to ALPGEN+HERWIG, we estimate the effect of hadronization uncertainties. Additional uncertainties on signal arise from color reconnection (CR), and initial and final state radiation (ISR/FSR) producing additional jets. The effect of CR is determined by comparing identical ALPGEN events interfaced to PYTHIA with two different tunes, Perugia 2011 and Perugia 2011NOCR. The effect of ISR/FSR is determined by modifying the factorization and renormalization scale implemented in the MC and more details can be found in [40].

2. *Parton distributions functions*

The uncertainty on the cross sections due to the uncertainty on PDFs is estimated following the procedure of Ref. [18] by reweighting the MC simulation according to each of the 20 pairs of error eigenvectors of the CTEQ6M PDF.

3. *Modeling of detector*

Uncertainties on the modeling of the detector include uncertainties on trigger efficiency, lepton identification and b -quark identification. The identification efficiencies for b , c , light quarks (u, d, s) and gluons in MC simulations are calibrated using dijet data [41], and variations within the calibration uncertainty are used to determine the systematic uncertainty due to b -quark identification. Additional uncertainties arise from track multiplicity requirements on the selected jets in the identification of b quarks.

Other instrumental uncertainties from modeling the detector arise from the calibration of the jet energy, resolution and efficiency. The jet energy scale (JES) corrects the measured energy of the jet to the energy of its constituent particles. The JES is derived using a quark-jet dominated γ + jet sample, and corrects for the difference in detector response between data and MC. An additional correction based on single particle response accounts for the different characteristics of quark and gluon jets. Jets in MC simulations have their transverse momenta smeared so that the simulated resolution matches the one observed in data. Calibrations to the jet reconstruction and identification efficiency in MC simulations are determined using Z/γ^* +jets data. As mentioned earlier jets are required to contain at least two tracks (see Sec. V), and in MC simulations the corresponding efficiency is adjusted to match the one derived in dijet data.

4. *Sample composition*

Uncertainties on the composition of the selected events arise from the heavy-flavor scale factor used for W +jets events, the assumed $t\bar{t}$ cross section, single top quark and diboson cross sections, and the estimate of the contributions from misidentified leptons. As introduced in Sec. VI, we determine a initial sample composition from a simultaneous fit to the MVA distribution in the $\ell + 2$ jets, $\ell + 3$ jets and $\ell + \geq 4$ jets samples. For this initial sample composition we assume an uncertainty of 5% on the normalization of the $t\bar{t}$ processes. This initial sample composition is only used to determine a systematic uncertainty on the contribution of W +jets processes. From the fit we derive a systematic uncertainty of $^{+3.5}_{-1.8}\%$ on the normalization of the Wlp +jets and $^{+17}_{-23}\%$ on the normalization of the $Wc\bar{c}$ + jets and $Wb\bar{b}$ + jets processes. An uncertainty of 20% on the Z/γ^* +jets cross section is assigned. The uncertainty on the single top quark cross sections is 12.6%, taken from varying the scale by factors of 2 and 0.5. An uncertainty of 7% on the diboson cross sections is assigned, corresponding to half the difference between the LO and NLO predictions. The uncertainties on the data-driven method of estimating multijet (MJ) background and its kinematic dependencies, mostly due to the uncertainties on the selection rates of true and false lepton candidates, are 40% in the μ +jets and 25% in the e +jets sample (including statistical component). These uncertainties are estimated by varying the contribution of $Wc\bar{c}$ + jets, $Wb\bar{b}$ + jets, $Zc\bar{c}$ + jets and $Zb\bar{b}$ + jets by $\pm 20\%$, the $t\bar{t}$ contribution by $\pm 10\%$, comparing the fake and true signal rates in different variables (quoting the largest difference as additional parametrization uncertainty). In addition, to estimate the contribution of the fake rate uncertainty, a different \cancel{E}_T cut of < 15 GeV (standard cut for the fake rate estimation is < 10 GeV) [35] is applied.

B. The $\ell\ell$ channel

In the following we describe the sources of systematic uncertainties studied in the $\ell\ell$ channel, which are mostly similar to those in the ℓ +jets channel. As discussed above, each source of systematic uncertainty yields a modified discriminant distribution of the b -ID MVA method and is used as a nuisance parameter in the fit to determine the $t\bar{t}$ production cross section in the $\ell\ell$ channel. The pre-fit systematic uncertainties are summarized in Table III, whereas the post-fit effects of the systematic uncertainties are summarized in Table IV.

1. Modeling of signal

The same sources of systematic uncertainties for the modeling of the signal as in the ℓ +jets decay channel are considered for the $\ell\ell$ channel as well. All uncertainties arising from the modeling of the signal are assumed to be 100% correlated between the ℓ +jets channel and the $\ell\ell$ channel.

2. Parton distributions functions

The uncertainty on the cross sections due to the uncertainty on PDFs is estimated following the same procedure as in the ℓ +jets case. The PDF uncertainty is assumed to be 100% correlated between the ℓ +jets and $\ell\ell$ channel.

3. Modeling of detector

The assigned uncertainties related to the modeling of the detector are the same as the ones assigned in the ℓ +jets channel and include uncertainties on the efficiencies of electron and muon identification, uncertainties on trigger efficiencies, the uncertainty in jet energy scale, jet energy resolution, jet identification efficiency, and b -quark jet tagging efficiency. All common uncertainties on the modeling of the detector, except uncertainties arising from modeling of the trigger, are assumed to be 100% correlated between the ℓ +jets and $\ell\ell$ channel.

4. Sample composition

The most significant contribution to the background related uncertainty in the $\ell\ell$ channel is from the uncertainty on instrumental background. We estimate this by changing the amount of instrumental background according to the uncertainty on its normalization. We also account for possible uncertainties in the distribution of instrumental background by changing the number of events in each bin of the of this instrumental background distribution by ± 1 standard deviation (SD) of its statistical uncertainty. Uncertainties from Z/γ^* +jets and diboson production are taken into account with the same procedure as in the ℓ +jets case. All common uncertainties on the sample composition, except uncertainties arising from the determination of the MJ background, are assumed to be 100% correlated between the ℓ +jets and $\ell\ell$ channel.

XI. FITTING PROCEDURE

As shown in Figs. 5 and 4, the MVA output distributions for the ℓ +jets and $\ell\ell$ channel provide a clear separation of signal and background events, which provides sensitivity to the $t\bar{t}$ signal contribution and to the most dominant background sources originating from W +jets contributions (ℓ +jets channel) or Z/γ^* +jets contributions ($\ell\ell$ channel).

We perform a simultaneous fit of MC templates to the data using the software package COLLIE (A Confidence Level Limit Evaluator) [42], which is widely used in D0 to provide confidence levels and evaluate exclusion limits, as well as to measure cross sections. In order to measure the cross section COLLIE performs a log-likelihood profile fit of MC templates to data using a nuisance parameter for every source of systematic uncertainty. This allows systematic uncertainties to influence the central value of the fit and allows a cross-calibration of the different systematic uncertainty sources in the several decay channels. The combination of the MVA topological method in the ℓ +jets channel with the b -ID MVA method in the $\ell\ell$ channel allows an improved cross-calibration of the different systematic uncertainties, where systematic uncertainties are either assumed to be fully correlated or not correlated (see Section X).

TABLE III: Sources of systematic uncertainties. The pre-fit uncertainty in percent from each source on the inclusive cross section is given for the ℓ +jets and the $\ell\ell$ channel. ‘‘Type’’ refers to a systematic uncertainty affecting the shape S or the normalization N of a distribution. The numbers presented for shape dependent uncertainties represent averages across the entire distribution.

Source of uncertainty	$\delta_{\ell+jets}^{\text{up}}, \%$	$\delta_{\ell+jets}^{\text{down}}, \%$	Type S/N	$\delta_{\ell\ell}^{\text{up}}, \%$	$\delta_{\ell\ell}^{\text{down}}, \%$	Type S/N
<i>Modeling of signal</i>						
Alternative signal model	+10	-10	S	+4	-4	S
Hadronization	+8	-8	S	+4	-4	S
Color reconnection	+2	-2	S	+2	-2	S
ISR/FSR variation	+2	-2	S	+2	-2	S
PDF	+7	-7	N	+1	-1	N
<i>Modeling of detector</i>						
Jet modeling & identification	+8	-8	S	+3	-3	S
b -jet modeling & identification	+5	-5	S	+12	-12	S
Lepton modeling & identification	+3.5	-3.5	S	+6	-6	N
Trigger efficiency	+5	-5	N	+2	-2	N
Luminosity	+4.7	-4.7	N	+4.3	-4.3	N
<i>Sample Composition</i>						
MC cross sections & branching ratios	+0.9	-0.9	N	+1.3	-1.3	N
Z/W p_T reweighting	+1.5	-1.5	S	+4	-4	S
Multijet contribution	+23	-23	S/N	+15	-15	S/N
Z/γ^* +jets scale factor	+25	-25	S/N	+2	-2	S/N
W +jets heavy flavor scale factor	+17	-23	S/N	<i>n.a.</i>	<i>n.a.</i>	<i>n.a.</i>
W +jets light parton scale factor	+3.5	-1.8	S/N	<i>n.a.</i>	<i>n.a.</i>	<i>n.a.</i>
MC statistics	<i>n.a.</i>	<i>n.a.</i>	<i>n.a.</i>	+3	-3	S/N

COLLIE models systematic uncertainties using a prior probability density function specified by ± 1 standard deviation of the nuisance parameter in question (see Eqn. 1). The prior distribution for each uncertainty was parametrized using a Gaussian distribution [42]. To evaluate systematic uncertainties the ± 1 SD inputs were propagated through the entire event selection. The description of systematic uncertainties can be found in Sec. X.

XII. CROSS SECTION DETERMINATION

Measurements involving top quarks benefit from the very short lifetime of the t quark, since it decays before it can hadronize. Effects of hadronization and QCD corrections are thus reduced. Moreover, at Tevatron energies the transverse momentum of $t\bar{t}$ pairs is almost always smaller than $m(t\bar{t})$ and production is central, so that almost the entire phase space of $t\bar{t}$ production is within the detector acceptance. Corrections to measured quantities as well as their uncertainties are therefore small, leading to well measured top-quark cross sections.

As introduced earlier we use a log-likelihood profile fit to determine the inclusive $t\bar{t}$ cross section $\sigma(t\bar{t})$. Equation 1 shows the definition of the combined likelihood, which includes prior probability densities on systematic uncertainties $\pi(\vec{\theta})$, and is based on the product of likelihoods for the individual channels, each of which is a product over histogram bins of a particular analysis channel.

$$\mathcal{L}(\vec{s}, \vec{b} | \vec{n}, \vec{\theta}) \times \pi(\vec{\theta}) = \prod_{i=1}^{N_C} \prod_{j=1}^{N_{\text{bins}}} \mu_{ij}^{n_{ij}} \frac{e^{-\mu_{ij}}}{n_{ij}!} \times \prod_{k=1}^{n_{\text{sys}}} e^{-\theta_k^2/2}. \quad (1)$$

The first product is over the number of channels (N_C) and the second product is over histogram bins containing n_{ij} events, binned in ranges of the final discriminants used for the individual analyses. The predictions for the bin contents are $\mu_{ij} = s_{ij}(\vec{\theta}) + b_{ij}(\vec{\theta})$ for channel i and histogram bin j , where s_{ij} and b_{ij} represent the expected SM signal and background in the bin. The predictions μ_{ij} include effects from limited detector resolution and efficiency, including those from trigger, selection and b -tagging efficiencies and for the kinematic and geometric acceptance.

Systematic uncertainties are parametrized by the dependence of s_{ij} and b_{ij} on $\vec{\theta}$. Each of the n_{sys} components of $\vec{\theta}$, θ_k , corresponds to a single independent source of systematic uncertainty scaled by its standard deviation, and each parameter may affect the predictions of several sources of signal and background in different channels, thus accounting for correlations.

TABLE IV: Sources of systematic uncertainties. The post-fit uncertainty from each source on the inclusive cross section is given for the combination. The last column shows the shifts in units of SD on the combined inclusive cross section due to a particular source.

Source of uncertainty	Uncertainties δ_{combined} , pb	Shift in units of σ
<i>Modeling of signal</i>		
Alternative signal model	± 0.09	+0.2
Hadronization	± 0.25	+0.7
Color reconnection	± 0.11	+0.2
ISR/FSR variation	± 0.06	-0.3
PDF	± 0.08	-0.5
<i>Modeling of detector</i>		
Jet modeling & identification	± 0.06	-0.3
b -jet modeling & identification	± 0.16	+1.3
Lepton modeling & identification	± 0.02	-0.7
Trigger efficiency	± 0.01	-0.2
Luminosity	± 0.20	+0.3
<i>Sample Composition</i>		
MC cross sections & branching ratios	± 0.03	+0.6
Z/W p_T reweighting	± 0.16	+0.9
Multijet contribution	± 0.09	+0.1
W +jets heavy flavor scale factor	± 0.15	-2.0
W +jets light parton scale factor	± 0.05	+0.8
MC statistics	± 0.01	< 0.0
Total systematic uncertainty	± 0.55	

XIII. CROSS SECTION RESULTS

As discussed in Sections XI and X we perform a simultaneous log-likelihood fit considering systematic uncertainties in the form of nuisance parameters. Thus correlations between the various decay channels are taken into account. Table IV summarizes the systematic uncertainties on the $t\bar{t}$ cross section in the ℓ +jets and $\ell\ell$ decay channels and for the combination. Individual sources of systematic uncertainty are added in quadrature. In addition we provide the ‘‘Shifts in units of SD’’, which refers to shifts on the combined inclusive cross section due to a particular source of systematic uncertainty (or nuisance parameter) relative to the central value of the combined $t\bar{t}$ cross section.

The combination of ℓ +jets and $\ell\ell$ channels using the topological discriminant and MVA b -jet method for the measurement of the inclusive cross section yields for a top quark mass of 172.5 GeV:

$$\sigma_{t\bar{t}} = 7.73 \pm 0.13 \text{ (stat.)} \pm 0.55 \text{ (syst.) pb,}$$

which corresponds to a relative total uncertainty of 7.3%.

Figure 6 shows the post-fit MVA topological discriminant distributions using the combined $t\bar{t}$ cross section. Similarly Fig. 7 shows the post-fit MVA b -ID discriminant distribution using the combined $t\bar{t}$ cross section. The result of the measurement in ℓ +jets channel when using the topological method is:

$$\sigma_{t\bar{t}} = 7.63 \pm 0.14 \text{ (stat.)} \pm 0.59 \text{ (syst.) pb,}$$

with a relative total uncertainty of 7.9%. For the $\ell\ell$ decay channel we employ the MVA b -jet method and measure:

$$\sigma_{t\bar{t}} = 7.60 \pm 0.34 \text{ (stat.)}^{+0.60}_{-0.58} \text{ (syst.) pb,}$$

with a relative total uncertainty of 9.0%. The inclusive $t\bar{t}$ production cross section can be compared to the fully resummed NNLL at NNLO QCD calculation (see Sec. III). The calculation yields for a top quark mass of 172.5 GeV an inclusive $t\bar{t}$ cross section of $\sigma_{\text{tot}}^{\text{res}} = 7.35^{+0.23}_{-0.27}$ (scale + pdf) pb.

The new D0 result is consistent with an earlier measurement by D0 using 5.3 fb⁻¹ of data [4] and supersedes the earlier results.

XIV. TOP QUARK POLE MASS

The mass of the top quark has been directly measured with a precision of less than 0.5% in a single measurement [45]. The Tevatron combination currently yields a top quark mass of 174.34 ± 0.64 GeV [3]. These direct measurements employed for the Tevatron combination are measuring the MC mass. Theoretical arguments suggest that the MC

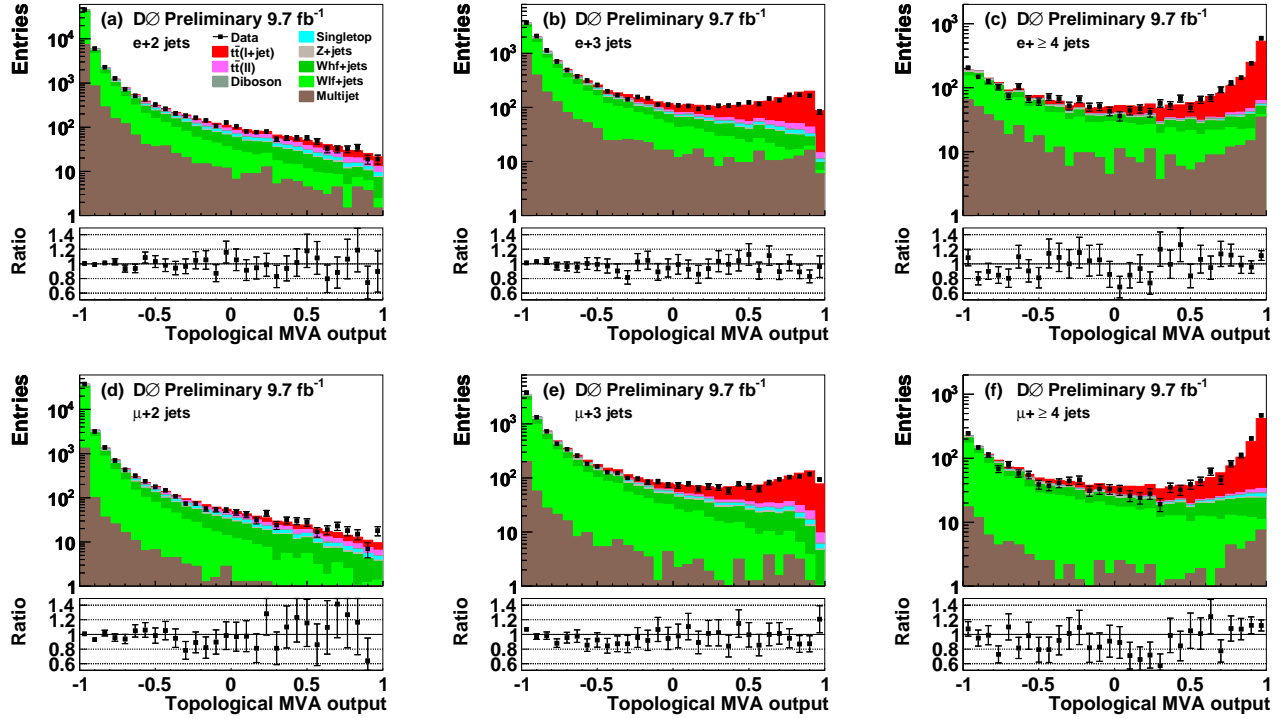


FIG. 6: Post-fit MVA topological discriminant distributions using the measured combined $t\bar{t}$ cross section for the (a) – (c) e +jets channel and for the (d) – (f) μ +jets channel in the two, three and inclusive four jet multiplicity bin.

mass as determined by these direct measurements of the top quark mass are within about 1 GeV to the well-defined pole mass of the top quark. An alternative measurement approach of the top quark mass is the extraction of the top quark mass by using the inclusive $t\bar{t}$ cross section. Comparing the top quark mass dependence of the inclusive $t\bar{t}$ cross section, as observed in the measurement, with the expected dependency in pQCD yields a theoretically well-defined top quark pole mass extraction.

TABLE V: The combined inclusive $t\bar{t}$ cross section as a function of the top quark mass with statistical and systematic uncertainties given separately.

Top quark mass [GeV]	Cross section $\sigma(t\bar{t})$ [pb]
150	10.53 ± 0.17 (stat.) $^{+0.78}_{-0.78}$ (syst.)
160	9.24 ± 0.16 (stat.) $^{+0.74}_{-0.74}$ (syst.)
165	8.07 ± 0.14 (stat.) $^{+0.65}_{-0.65}$ (syst.)
170	8.28 ± 0.14 (stat.) $^{+0.57}_{-0.57}$ (syst.)
172.5	7.73 ± 0.13 (stat.) $^{+0.55}_{-0.55}$ (syst.)
175	7.80 ± 0.13 (stat.) $^{+0.51}_{-0.51}$ (syst.)
180	7.42 ± 0.13 (stat.) $^{+0.50}_{-0.50}$ (syst.)
185	6.92 ± 0.12 (stat.) $^{+0.45}_{-0.45}$ (syst.)
190	6.85 ± 0.12 (stat.) $^{+0.43}_{-0.43}$ (syst.)

Table V presents the combined inclusive $t\bar{t}$ cross section as a function of the top quark mass. Each individual mass point is a separate combined log-likelihood fit of the ℓ +jets and $\ell\bar{\ell}$ channel MVA discriminant inputs, as it was done for the mass point of 172.5 GeV. Figure 8 shows the measured and expected mass dependency of the top quark pair production cross section. For the measured dependency we provide a cubic fit to the individual cross section

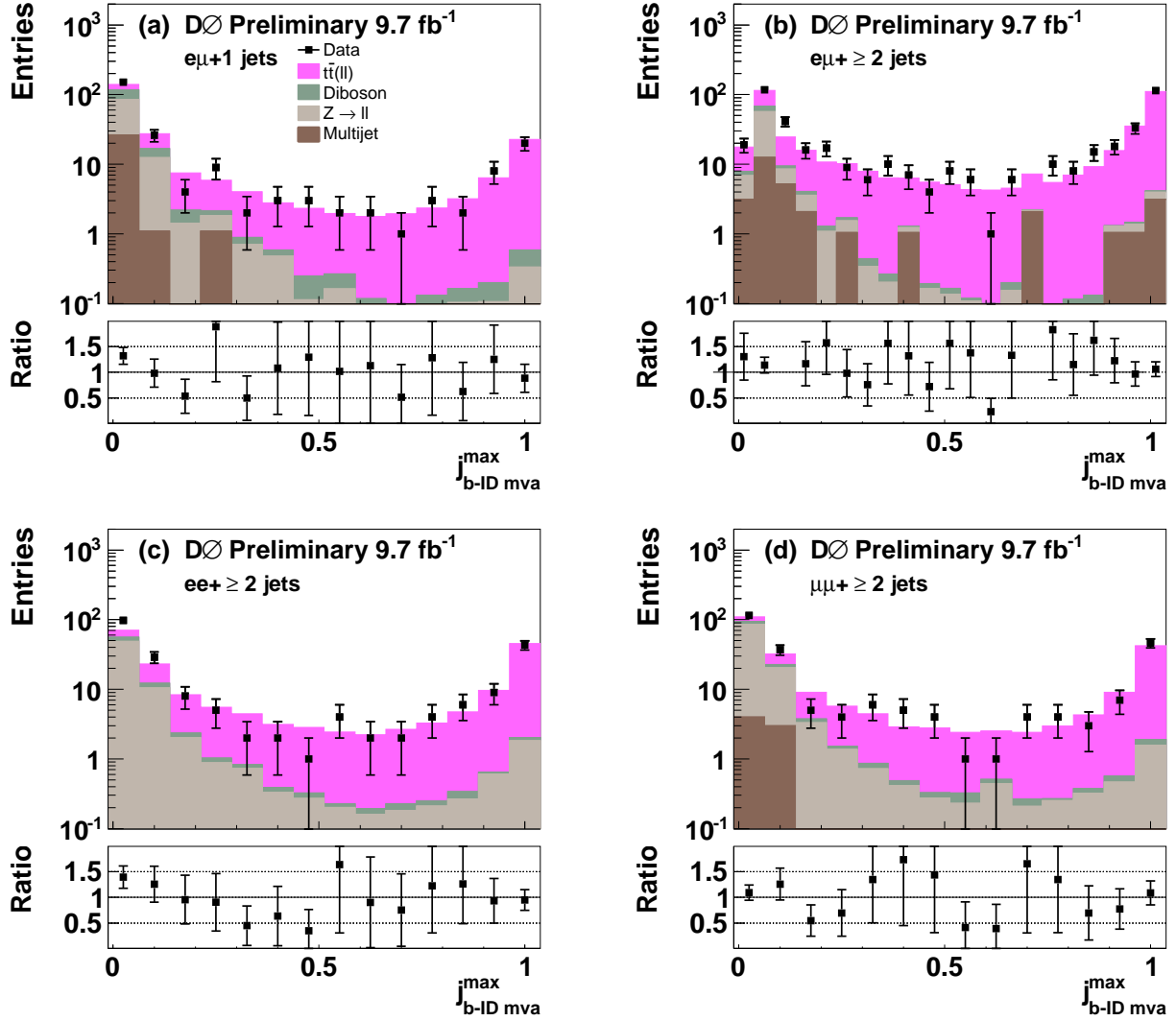


FIG. 7: Resulting postfit MVA output 1D-histograms are shown. Histograms are shown with respect to lepton type and number of jets in the event. Numbers in legend correspond to expected number of events from after the fit sample.

measurements at various mass points (see Table V). Uncertainties on the measured value include statistical and all systematic uncertainties as discussed in Sec. X and are indicated as hashed band.

To determine the top quark pole mass from the inclusive $t\bar{t}$ cross section we parametrize the experimentally measured slope with a cubic function. The difference to a quadratic function is negligible. Following the method in [46], we extract the most probable m_t value and uncertainty by employing a normalized joint-likelihood function, which takes into account the total experimental uncertainty and theoretical uncertainties on renormalization and factorization scale variations, and PDF uncertainties. Employing the cubic parametrization and the theory predictions at NNLO pQCD we determine a pole mass of the top quark of:

$$m_t = 169.5_{-3.4}^{+3.3} (\text{tot.}) \text{ GeV}. \quad (2)$$

The precision of this determination is 1.9%, and represents the most precise determination of the top quark pole mass from the inclusive $t\bar{t}$ cross section at the Tevatron. This precision can be compared to the previous D0 determination that had a precision of 3% [46].

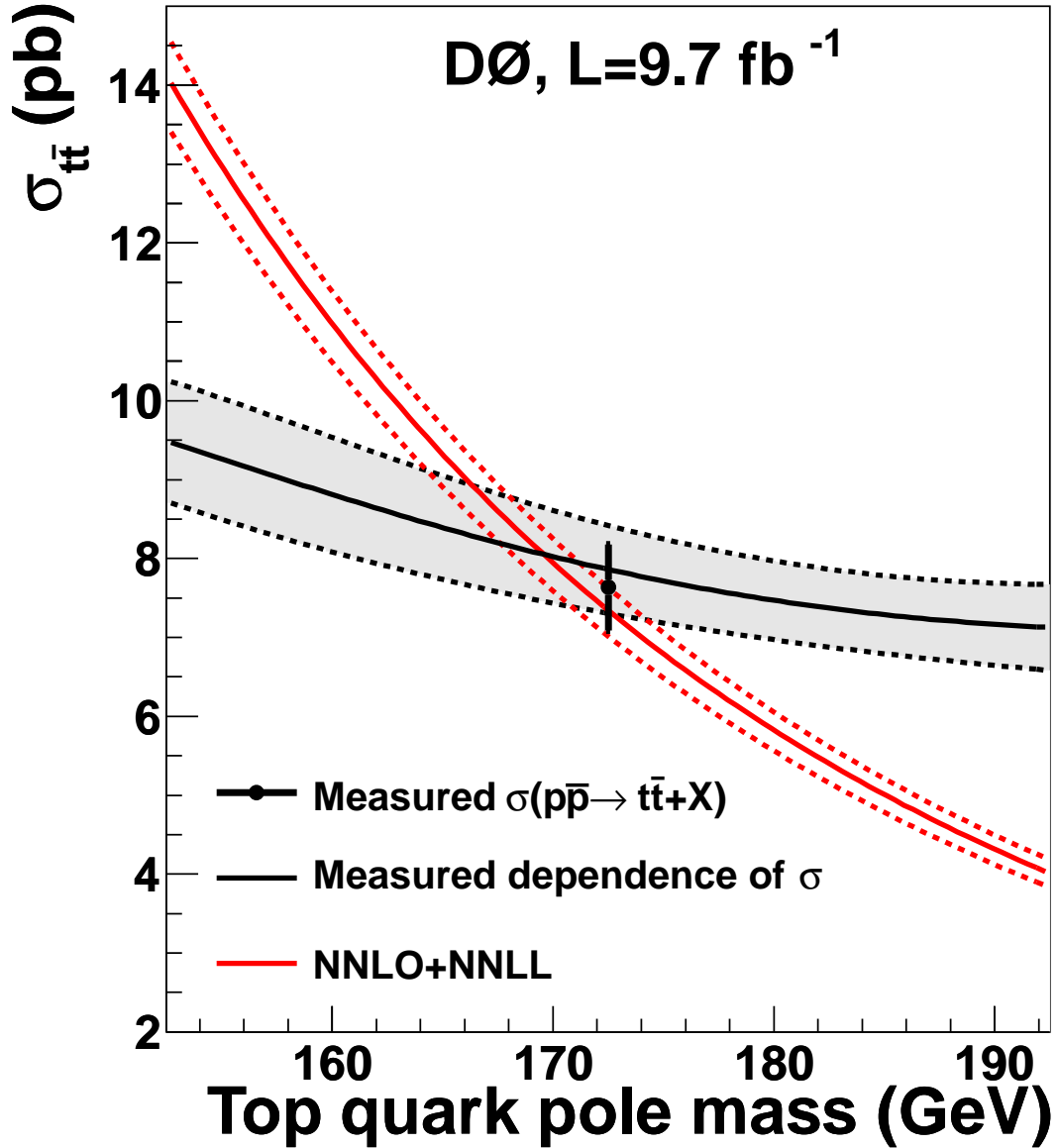


FIG. 8: The measured $t\bar{t}$ production cross section dependency on the top quark mass compared to the one provided by the NNLO pQCD calculation TOP++ [44], which implements pQCD calculations according to [19].

XV. CONCLUSIONS

The inclusive $t\bar{t}$ production cross section has been measured combining the ℓ +jets and dilepton decay channel based on the full Tevatron data set for these kind of measurements at $\sqrt{s} = 1.96$ TeV. The data are corrected for detector efficiency and acceptance. For a top quark mass of 172.5 GeV we measure:

$$\sigma_{t\bar{t}} = 7.73 \pm 0.13 \text{ (stat.)} \pm 0.55 \text{ (syst.) pb,}$$

which corresponds to a relative uncertainty of 7.3%.

The measured inclusive cross sections are in general agreement with predictions by QCD. We determine a pole mass of the top quark of $m_t = 169.5^{+3.3}_{-3.4}$ (tot.) GeV, which corresponds to a precision of 1.9% and represents the most precise determination of the top quark pole mass at the Tevatron.

XVI. ACKNOWLEDGMENTS

We thank the staffs at Fermilab and collaborating institutions, and acknowledge support from the Department of Energy and National Science Foundation (United States of America); Alternative Energies and Atomic Energy Commission and National Center for Scientific Research/National Institute of Nuclear and Particle Physics (France); Ministry of Education and Science of the Russian Federation, National Research Center “Kurchatov Institute” of the Russian Federation, and Russian Foundation for Basic Research (Russia); National Council for the Development of Science and Technology and Carlos Chagas Filho Foundation for the Support of Research in the State of Rio de Janeiro (Brazil); Department of Atomic Energy and Department of Science and Technology (India); Administrative Department of Science, Technology and Innovation (Colombia); National Council of Science and Technology (Mexico); National Research Foundation of Korea (Korea); Foundation for Fundamental Research on Matter (The Netherlands); Science and Technology Facilities Council and The Royal Society (United Kingdom); Ministry of Education, Youth and Sports (Czech Republic); Bundesministerium für Bildung und Forschung (Federal Ministry of Education and Research) and Deutsche Forschungsgemeinschaft (German Research Foundation) (Germany); Science Foundation Ireland (Ireland); Swedish Research Council (Sweden); China Academy of Sciences and National Natural Science Foundation of China (China); and Ministry of Education and Science of Ukraine (Ukraine).

-
- [1] CDF Collaboration, F. Abe *et al.*, Phys. Rev. Lett. **74**, 2626 (1995).
 - [2] D0 Collaboration, S. Abachi *et al.*, Phys. Rev. Lett. **74**, 2632 (1995).
 - [3] CDF & D0 Collaboration, V. M. Abazov *et al.*, Phys. Rev. D **86**, 092003 (2012), updated in [arxiv:1407.2682].
 - [4] D0 Collaboration, V. M. Abazov *et al.*, Phys. Rev. D **84**, 012008 (2011).
 - [5] CDF Collaboration, F. Abe *et al.*, Phys. Rev. D **88**, 091103 (2013).
 - [6] CMS Collaboration, S. Chatrchyan *et al.*, J. High Energy Phys. 02 (2014) 024.
 - [7] ATLAS Collaboration, G. Aad *et al.*, Phys. Rev. D **91**, 112013 (2015).
 - [8] K. Kondo, J. Phys. Soc. Jap. **57**, 4126 (1988); R. M. Neal, Bayesian Learning for Neural Networks (Springer-Verlag, New York, 1996); L. Breiman *et al.*, Classification and Regression Trees (Wadsworth, Stamford, 1984).
 - [9] A. Hoecker, P. Speckmayer, J. Stelzer, J. Therhaag, E. von Toerne, and H. Voss, PoS ACAT **040** (2007).
 - [10] D0 Collaboration, V. M. Abazov *et al.*, Nucl. Instrum. Methods Sect. A **763**, 290 (2014).
 - [11] R. Brun and F. Carminati, CERN Program Library Long Writeup W5013 (1993) (unpublished).
 - [12] S. Frixione and B. R. Webber, J. High Energy Phys. 06 (2002) 029; S. Frixione *et al.*, J. High Energy Phys. 08 (2003) 007.
 - [13] M. L. Mangano *et al.*, J. High Energy Phys. 07 (2003) 001.
 - [14] E. E. Boos, V. E. Bunichev *et al.*, Physics of Atomic Nuclei, 780 (2006).
 - [15] G. Corcella *et al.*, J. High Energy Phys. 01 (2001) 010.
 - [16] T. Sjöstrand, S. Mrenna, and P. Skands, J. High Energy Phys. 05 (2006) 026.
 - [17] J. Pumplin *et al.*, J. High Energy Phys. 07 (2002) 12.
 - [18] J. Pumplin *et al.*, J. High Energy Phys. 10 (2003) 46.
 - [19] P. Barnreuther, M. Czakon and A. Mitov, Phys. Rev. Lett. **109** 132001 (2012).
 - [20] N. Kidonakis, Phys. Rev. D **90**, 014006 (2014).
 - [21] A. D. Martin, W. J. Stirling, R. S. Thorne and G. Watt, Eur. Phys. J. C **63**, 189 (2009).
 - [22] J. Campell, R. K. Ellis, Nucl. Phys. Proc. Suppl. **10** 205 (2010).
 - [23] D0 Collaboration, V. M. Abazov *et al.*, Phys. Lett. B **693**, 522 (2010).
 - [24] C. Balazs and C. P. Yuan, Phys. Rev. D **56**, 5558 (1997).
 - [25] N. Kidonakis, Phys. Rev. D **74**, 114012 (2010).
 - [26] D0 Collaboration, V. M. Abazov *et al.*, Nucl. Instrum. Methods Sect. A **565**, 463 (2006).
 - [27] S. N. Ahmed *et al.*, Nucl. Instrum. Methods Sect. A **634**, 8 (2011).
 - [28] R. Angstadt *et al.*, Nucl. Instrum. Methods Sect. A **622**, 298 (2010).
 - [29] V. M. Abazov *et al.*, Nucl. Instrum. Methods in Phys. Res. Sect. A **552**, 372 (2005).
 - [30] T. Andeen *et al.*, FERMILAB-TM-2365 (2007).
 - [31] M. Abolins *et al.*, Nucl. Instrum. Methods in Phys. Res. Sect. A **584**, 75 (2008).
 - [32] D0 Collaboration, V. M. Abazov *et al.*, Phys. Rev. Lett. **101**, 062001 (2008).
 - [33] D0 Collaboration, V. M. Abazov *et al.*, Nucl. Instrum. Methods Sect. A **737**, 281 (2014).
 - [34] D0 Collaboration, V. M. Abazov *et al.*, submitted to Nucl. Instrum. Methods Sect. A [arXiv:hep-ph/1401.0029] (2013).
 - [35] D0 Collaboration, V. M. Abazov *et al.*, Phys. Rev. D **90**, 092006 (2014).
 - [36] D0 Collaboration, V. M. Abazov *et al.*, Phys. Rev. D **88**, 112002 (2013).
 - [37] D0 Collaboration, V. M. Abazov *et al.*, Phys. Rev. D **74**, 112004 (2006).
 - [38] S. Moch and P. Uwer, Phys. Rev. D **78**, 034003 (2008).
 - [39] D0 Collaboration, submitted to PRD (2015).
 - [40] D0 Collaboration, V. M. Abazov *et al.*, Phys. Rev. D **91**, 112003 (2015).
 - [41] D0 Collaboration, V. M. Abazov *et al.*, Phys. Rev. D **84**, 032004 (2011).

- [42] CDF & D0 Collaboration, V. M. Abazov *et al.*, Phys. Rev. D **88**, 052014 (2013).
- [43] J. Beringer *et al.* (Particle Data Group), Phys. Rev. D **86**, 010001 (2012).
- [44] M. Czakon and A. Mitov, Computer Physics Communications **185** 2930 (2014).
- [45] D0 Collaboration, V. M. Abazov *et al.*, Phys. Rev. Lett. **113**, 032002 (2014).
- [46] D0 Collaboration, V. M. Abazov *et al.*, Phys. Lett. B **703**, 422 (2011).

Appendix A: Variables selected for the topological discriminant

The 28 variables selected for the MVA topological method employed to measure the $t\bar{t}$ production cross section in the $\ell + \text{jets}$ decay channel. The list given below is sorted according to the ranking provided by the BDTG method.

- $j_{b\text{-ID MVA}}^{\max}$: The maximum output value of the MVA b -jet discriminant of a jet.
- H_T^3 : The scalar sum of transverse momenta of jets starting with the 3rd jet multiplicity bin.
- $H_T^{2,0}$: The scalar sum of transverse momenta of jets satisfying $|\eta| < 2.0$.
- $j_{b\text{-ID MVA}}^{\text{lead.}}$: The b – ID MVA value of the leading jet.
- Centrality \mathcal{C} : Ratio of the scalar sum of the transverse momentum of all jets to the energy of all jets.
- H_T : The scalar sum of the transverse momenta of all jets, the lepton and \cancel{E}_T .
- p_T^i : The transverse momenta of the individual jets i .
- $j_{b\text{-ID MVA}}^{2\text{ndlead.}}$: The b – ID MVA value of the second leading jet.
- H_T^ℓ : The scalar sum of the transverse momenta of all jets and the lepton.
- Sphericity \mathcal{S} : Similar to \mathcal{A} this variable is based on \mathcal{A} as well and defined as $\mathcal{S} = \frac{3}{2}(\lambda_2 + \lambda_3)$.
- $m(t\bar{t})$: The invariant mass of the $t\bar{t}$ pair. The energy of the neutrino is determined by constraining the invariant mass of the lepton and vector \cancel{E}_T (as the neutrino) to the mass of the W boson. Of the two possible solutions for the longitudinal momentum of the neutrino, we use the one with the smaller absolute value.
- η^{j^1} : The rapidity of the leading jet.
- $\Delta R(j^1, j^2)$: The separation in the distance R between the leading and second leading jet.
- p_T^W : The transverse momentum of the reconstructed W boson, which decays hadronically.
- $M_T^{j^2\nu\ell}$: The transverse mass of the system consisting of the second leading jet, the neutrino and the lepton.
- Aplanarity \mathcal{A} : Diagonalizing the normalized quadratic momentum tensor \mathcal{M} yields three eigenvalues λ_i [4] and the Aplanarity is defined as $\mathcal{A} = \frac{3}{2}\lambda_3$ and reflects the degree of isotropy of an event.
- $\Delta R(j^1, j^i)$: The separation in the distance R between the leading and all other jet.
- m_{jet} : The invariant mass of the jets.
- M_T^{jet} : The transverse mass of the first two leading jets.
- $M_{j^2\nu\ell}$: The invariant mass of the system consisting of the second leading jet, the neutrino and the lepton.
- $\Delta\phi(\ell, \cancel{E}_T)$: The separation in azimuth between the lepton and the direction of \cancel{E}_T .
- \cancel{E}_T : Missing transverse momentum.
- η^{lepton} : The rapidity of the lepton.
- $\Delta\phi(j^1, j^i)$: The minimum separation in azimuth between the leading and any other jet.
- $\cancel{E}_T^{\text{perp}}$: Missing transverse momentum perpendicular to the direction of the lepton.